Title Page

MYH11 rare variant augments aortic growth and induces cardiac hypertrophy and heart failure with pressure overload

Zhen Zhou[1], Kgosi Hughes[1], Nisha Saif[1,2], Hyoseon Kim[3], Michael P. Massett[3], Mingjie Zheng[4], Alana C. Cecchi[1], Dongchuan Guo[1], David R. Murdock[1], Ping Pan[1], Jelita S. Clinton[1], Jun Wang[4], John M. Greally[5], Dianna M. Milewicz[1]

[1]Division of Medical Genetics, Department of Internal Medicine, The University of Texas Health Science Center at Houston McGovern Medical School, Houston, TX, USA.

[2]Broad Institute of MIT and Harvard, Cambridge, MA, USA.

[3]Department Kinesiology & Sport Management, Texas Tech University, Lubbock, TX, USA.

[4]Department of Pediatrics, The University of Texas Health Science Center at Houston McGovern Medical School, Houston, TX, USA.

[5]Department of Genetics, Albert Einstein College of Medicine, NY, USA.

Correspondence: Dianna.M.Milewicz@uth.tmc.edu, +1 713-500-6715,

Division of Medical Genetics, Department of Internal Medicine, McGovern Medical School, The University of Texas Health Science Center at Houston, 6431 Fannin Street, MSB 6.100, Houston, TX 77030, USA

Abstract

Smooth muscle cell-specific myosin heavy chain, encoded by *MYH11*, is selectively expressed in smooth muscle cells (**SMC**s). Pathogenic variants in *MYH11* predispose to a number of disorders, including heritable thoracic aortic disease associated with patent ductus arteriosus, visceral myopathy, and megacystis-microcolon-intestinal hypoperistalsis syndrome. Rare variants of uncertain significance occur throughout the gene, including *MYH11* p.Glu1892Asp, and we sought to determine if this variant causes thoracic aortic disease in mice. Genomic editing was used to generate *Myh11*$^{E1892D/E1892D}$ mice. Wild-type (**WT**) and mutant mice underwent cardiovascular phenotyping and with transverse aortic constriction (**TAC**). *Myh11*$^{E1892D/E1892D}$ and WT mice displayed similar growth, blood pressure, root and ascending aortic diameters, and cardiac function up to 13 months of age, along with similar contraction and relaxation on myographic testing. TAC induced hypertension similarly in *Myh11*$^{E1892D/E1892D}$ and WT mice, but mutant mice showed augmented ascending aortic enlargement and increased elastic fragmentation on histology. Unexpectedly, male *Myh11*$^{E1892D/E1892D}$ mice two weeks post-TAC had decreased ejection fraction, stroke volume, fractional shortening, and cardiac output compared to similarly treated male WT mice. Importantly, left ventricular mass increased significantly due to primarily posterior wall thickening, and cardiac histology confirmed cardiomyocyte hypertrophy and increased collagen deposition in the myocardium and surrounding arteries. These results further highlight the clinical heterogeneity associated with *MYH11* rare variants. Given that *MYH11* is selectively expressed in SMCs, these results implicate a role of vascular SMCs in the heart contributing to cardiac hypertrophy and failure with pressure overload.

Author Summary

In this study, we explore the impact of a specific genetic variant, *MYH11* p.Glu1892Asp, on the heart and blood vessels in mice. The *MYH11* gene is crucial for smooth muscle cells, which are found in the walls of blood vessels and play an important role in various vascular diseases. We created mice with this genetic variant to see if it would lead to thoracic aortic disease, a condition affecting the main artery from the heart. We found that mice with the variant were similar to normal mice in many aspects, such as growth, blood pressure, and heart function, for up to 13 months. However, when we induced high blood pressure in the mice, the mutant mice showed more significant enlargement of the aorta and damage to the elastic fibers in the aortic walls. Interestingly, male mutant mice also developed heart problems, such as reduced heart pumping ability and increased heart muscle thickness, after the high blood pressure challenge. This was accompanied by signs of heart muscle cell enlargement and increased tissue stiffness. These findings suggest that this rare *MYH11* variant can contribute to a range of heart and vascular issues, particularly under conditions of pressure overload, and highlight the importance of smooth muscle cells in the development of these problems.

Introduction

MYH11 encodes the smooth muscle-specific isoform of myosin heavy chain (**SMMHC**), which associates with a regulatory light chain and a second light chain of unknown function and polymerizes to form the thick filament in the contractile unit of smooth muscle cells (**SMC**s) [1]. *MYH11* is only expressed in SMCs, as illustrated by the fact that the *Myh11* promoter is used as a Cre-driver to lineage-trace SMCs [2-6]. Pathogenic variants in *MYH11* confer a highly penetrant risk for several disorders, including heritable thoracic aortic disease associated with patent ductus arteriosus [7-11]. Although rare missense variants are present throughout *MYH11*, the majority of pathogenic variants that cause heritable thoracic aortic disease are large, in-frame deletions in the coiled-coil domain, a region that is critical for polymerization of SMMHC into thick filaments. Rare chromosomal duplications of 16p13.1 that include *MYH11* and eight other genes also confer an increased risk for aortic dissection. However, there is no evidence that the corresponding deletion increases the risk for thoracic aortic disease (**TAD**) [12]. Instead, recessive loss-of-function *MYH11* pathogenic variants are responsible for fetal megacystis-microcolon. Finally, heterozygous variants that disrupt the termination codon at the C-terminus and add extra amino acids to the end of the protein predispose individuals to a smooth muscle dysmotility syndrome with esophageal, gastric, and intestinal complications [13-15].

MYH11 variants of uncertain significance (**VUS**s) are commonly reported with genetic testing, but the phenotypic variability and burden of *MYH11* rare variants make it difficult to assign pathogenicity to identified variants. We previously determined that a VUS in *MYH11,* p.Arg247Cys (R247C), decreases myosin motor function in *in vitro* assays [16]. *Myh11*$^{R247C/R247C}$ mice show decreased aortic ring contraction, yet have normal growth, survival, and no evidence of TAD [16]. However, when hypertension is induced using 3g/L L-N^{G}-Nitro arginine methyl ester

and a high-salt diet, one-fifth of *Myh11*$^{R247C/R247C}$ mice die due to acute dissection of the proximal aorta (manuscript submitted). More recently, a heterozygous in-frame deletion in *MYH11*, p.Lys1256del, segregated with thoracic aortic dissection in two independent pedigrees [9]. The homozygous p.Lys1256del mice also had no evidence of aortic disease up to 18 months of age, but aortic dissection rates are higher in both heterozygous and homozygous mutant mice with angiotensin II infusion compared to similarly treated wild-type (**WT**) mice [17]. These data support that rare variants in *MYH11* can contribute to increased risk for TAD.

MYH11 missense VUSs in the coiled-coil region have not been functionally assessed in mice, so we sought to determine if *MYH11,* p.Glu1892Asp (E1892D) increases the risk for TAD in a mouse model. *Myh11*$^{E1892D/E1892D}$ mice did not develop TAD with age, but when male *Myh11*$^{E1892D/E1892D}$ mice were subjected to transverse aortic constriction (**TAC**) for 2 weeks, augmented ascending aortic enlargement occurred when compared to WT mice. Unexpectedly, TAC also induced significant cardiomyocyte hypertrophy, increased cardiac fibrosis, and impaired left ventricular contractile function in the *Myh11*$^{E1892D/E1892D}$ mice. These studies broaden our understanding of the phenotypes associated with *MYH11* rare variants and identify a novel role for mutant arterial SMCs contributing to aberrant cardiac remodeling with pressure overload in mice.

Results

VUS in *MYH11*, p.Glu1892Asp, identified in a patient with TAD

The proband is a 66-year-old male of European descent with an aortic root that progressively increased from 4.2 to 4.8 cm over 10 years, and he underwent a successful valve-sparing aortic root and ascending aorta repair. The proband has pectus excavatum, pes planus, and myopia, but no other skeletal, cardiac, or ocular abnormalities. He also has hypercholesterolemia

and hypertension that are controlled with medications. His father had a 4.2 cm aortic root and died of lung cancer at the age of 68 years, and his paternal grandfather died suddenly of an unknown cause at the age of 50 years. There was no other family history of TAD or sudden death.

Genome sequencing performed on DNA isolated from both peripheral blood leukocytes and tissues from the resected aorta showed no evidence of pathogenic variants in known aortopathy genes, but revealed a VUS in *MYH11,* p.Glu1892Asp (c.5676G>C; CADD score 23.70 and REVEL score 0.562). The variant is located at the C-terminus in the α-helical coiled-coil domain and occurs in the gnomAD database at a frequency of ~0.6% in European populations, ~0.2% in South Asian and African/African-American populations, and is not found in East Asian populations. The relatively high frequency of the variant led to the categorization as benign or likely benign in Clinvar (VCV000138358.34).

Validation and cardiovascular phenotyping of *Myh11*$^{E1892D/E1892D}$ mice

The *Myh11* p.E1892D variant was introduced using CRISPR/Cas editing of C57BL/6J embryos. Sequencing of mouse tail DNA and cDNA from both heart and thoracic aortic tissues confirmed the *Myh11* variant was present in genomic DNA and the expressed transcript (**Fig 1A**). A synonymous missense variant, p.Ser1893Ser (c.5679C>A), was also identified in the genomic DNA, but it did not alter mRNA splicing based on SpliceAI analysis. A total of 102 progenies from heterozygous breeders were screened, and expected Mendelian ratios of the variant were obtained (**S2 Table**).

Myh11$^{E1892D/E1892D}$ mice and littermate controls (10 males and 10 females) routinely underwent cardiovascular phenotyping every 6 weeks up to 13 months of age. *Myh11*$^{E1892D/E1892D}$ mice grew normally and maintained similar blood pressure to WT mice. Cardiovascular

assessment found that blood pressure and growth of root and ascending aorta did not differ between the *Myh11*$^{E1892D/E1892D}$ and WT mice, with the exception of significant enlargement of ascending aorta in older female *Myh11*$^{E1892D/E1892D}$ mice compared to female WT mice (**Fig 1B-C**). Left ventricular contractile function was assessed, and similar ejection fraction and fractional shortening were observed in the WT and mutant mice (**Fig 1D**).

To evaluate SMC contractility in the aortas, the isometric force of ascending aortic rings in response to contractile agonists and vasodilators was measured using aortas from male and female WT and *Myh11*$^{E1892D/E1892D}$ mice at 10 months of age. The contractile tension development and the maximum force generation in response to phenylephrine or potassium chloride showed no difference between *Myh11*$^{E1892D/E1892D}$ and WT aortas (**Fig 2A**). A similar level of arterial relaxation was also found in response to acetylcholine or sodium nitroprusside (**Fig 2A**). Immunoblotting of protein lysates of the ascending aortas showed no difference of SMC contractile markers among WT, *Myh11*$^{E1892D/+}$, and *Myh11*$^{E1892D/E1892D}$ aortas (**Fig 2B**).

Pressure overload augments ascending aortic enlargement in *Myh11*$^{E1892D/E1892D}$ mice

We previously demonstrated that proximal aorta enlarges two weeks after TAC in WT C57BL/6J mice and is associated with aortic medial and adventitial thickening [18]. *Myh11*$^{E1892D/E1892D}$ and WT mice of both sexes were subjected to TAC surgeries at 10-12 weeks of age. Mortality rates immediately following recovery from anesthesia were similar across the four groups: 22% (2/9) for male WT, 30% (3/10) for male mutants, 30% (3/10) for female WT, and 20% (2/10) for female mutants. These deaths were associated with acute congestive heart failure due to the constriction. Additionally, one female mutant mouse died of a ruptured left main coronary artery and cardiac tamponade one day after TAC, and one male mutant mouse died of congestive

heart failure on day eight (**S1 Fig** and **S1 Table**). Two weeks post-surgery, both male and female *Myh11*$^{E1892D/E1892D}$ mice exhibited significant increases in the ascending aortic diameter compared to WT TAC mice, despite displaying comparable levels of systolic and diastolic blood pressure (**Fig 3A-B** and **S2A-B Figs**). Histology analysis revealed significant increases in medial thickening and the number of elastic breaks in the mutant aortas compared to WT aortas, with no difference in adventitial area or collagen accumulation (**Fig 3A** and **3C**).

Pressure overload induces left ventricular posterior wall hypertrophy and heart failure in male *Myh11*$^{E1892D/E1892D}$ mice

TAC increases cardiac afterload and is routinely used to study cardiac hypertrophy and heart failure [19]. Unexpectedly, male *Myh11*$^{E1892D/E1892D}$ mice undergoing TAC had significantly impaired left ventricular contractile function by echocardiographic studies two weeks after TAC, as illustrated by the decreased ejection fraction, stroke volume, fractional shortening, and cardiac output in these mutant mice compared to similarly treated male WT mice (**Fig 4A-B**); these changes were not present in the female mutant mice compared to female WT mice (**S2C Fig**). Subsequent evaluation revealed that TAC induced a significant increase in left ventricular mass in male *Myh11*$^{E1892D/E1892D}$ mice compared to male WT TAC mice, primarily characterized by posterior wall thickening (**Fig 4C**). Additionally, both end-systolic and end-diastolic diameters and volumes of the left ventricle were significantly enlarged in male *Myh11*$^{E1892D/E1892D}$ mice (**Fig 4C**). In contrast, alterations of these cardiac remodeling were not observed in female *Myh11*$^{E1892D/E1892D}$ mice after TAC, except those limited exclusively to the left ventricular end-diastolic diameter when compared to WT female mice (**S2D Fig**).

Heart tissue obtained from male WT and *Myh11*$^{E1892D/E1892D}$ mice post-TAC underwent WGA staining [20, 21]. The cardiomyocyte cross-sectional area in the posterior wall of the left

ventricle corroborated significant cardiomyocyte hypertrophy in the *Myh11*$^{E1892D/E1892D}$ heart compared to WT hearts, while no difference was observed between the anterior walls (**Fig 4D** and **S3 Fig**). Quantification for collagen deposition showed increased peri-arterial and left ventricular posterior wall fibrosis in the *Myh11*$^{E1892D/E1892D}$ hearts compared to WT group (**Fig 4E**).

Discussion

A missense VUS in the coiled-coil domain of *MYH11*, p.Glu1892Asp, was identified in a proband with aortic root aneurysm. The functional impact of this variant was investigated by introducing it into the mouse genome. Similar to other mouse models of genetic variants predisposing to TAD [16, 17], *Myh11*$^{E1892D/E1892D}$ mice develop normally without thoracic aortic enlargement, but increasing the forces on the aorta via TAC augments ascending aortic enlargement in *Myh11*$^{E1892D/E1892D}$ mice compared to similarly treated WT mice. *MYH11*, p.K1256del, is a pathogenic variant that causes an autosomal dominant inheritance of a predisposition for type A and B dissections [9]. Although there is no evidence of TAD in mice heterozygous or homozygous for this variant, angiotensin II infusion induces both thoracic and abdominal aortic dissections in both heterozygous and homozygous mice [17]. Thus, these data support that the *MYH11*, p.Glu1892Asp, variant increases the risk for TAD, but further data are needed to determine the penetrance and additional genetic or environmental factors that contribute to the penetrance of TAD associated with this variant.

An unexpected finding in this study is the sex-dependent aberrant cardiac remodeling observed in *Myh11*$^{E1892D/E1892D}$ mice with pressure overload, as evidenced by the increased cardiomyocyte hypertrophy, posterior wall thickening and left ventricle failure following TAC. TAC is a well-established model to mimic hypertensive heart failure in humans, particularly

replicating cardiac hypertrophy and subsequent heart failure [22]. *MYH11* expression is the most specific marker of SMCs identified to date and it is not expressed in other cell types, including myofibroblasts [2-6]. Thus, our data indicate that a rare variant in a gene expressed exclusively in SMCs can trigger increased cardiomyocyte hypertrophy and decreased left ventricular contractile function, implicating a novel role for arterial SMCs in driving pathologic cardiac remodeling with pressure overload, in this case in a sex-specific manner. Pathogenic variants in *FBN1*, which encodes fibrillin-1, a protein that is a major component of extracellular matrix microfibrils, are the cause of Marfan syndrome, a genetic disorder characterized by TAD, skeletal, and ocular abnormalities. Although pathogenic variants in *FBN1* are associated with an increased risk for dilated cardiomyopathy in both patients and mice, *FBN1* is expressed in many tissues, including SMCs, cardiomyocytes, and cardiac fibroblasts [23].

In this model, constriction of the transverse aorta leads to increased pressure load on the left ventricle, triggering a cascade of molecular events similar to those observed in clinical conditions such as poorly controlled hypertension or aortic stenosis. Studies utilizing the TAC mouse model to study the mechanisms underlying cardiac remodeling and pump failure need to consider the genetic background [24, 25], degree and duration of constriction [26, 27], and sex [28, 29]. Male C57BL/6J mice undergoing TAC using a 27-gauge needle develop cardiac hypertrophy and pump failure as early as 7 days after surgery, which are characterized by increased mass of left ventricle, thicknesses of septal and posterior wall, along with decreased ejection fraction and fractional shortening [26]. In the current study, we replicate the decreased left ventricular contractile function in male WT mice 2 weeks after surgery using a 27-gauge needle [18], and identify further decline of heart contraction in male *Myh11*$^{E1892D/E1892D}$ mice. It has been reported that TAC-induced cardiac hypertrophy and impaired contraction show sex differences 6 weeks

after TAC in C57BL/6J WT mice [29]. However, in this study, both ejection fraction and fractional shortening are significantly decreased in male versus female *Myh11*$^{E1892D/E1892D}$ mice just 2 weeks after surgery, indicating a rapid decline of left ventricular contractile function in male *Myh11*$^{E1892D/E1892D}$ mice (**S4 Fig**). When female mice lacking estrogen receptor beta gene (*Esr2*$^{-/-}$) are subjected to TAC for 2 weeks, a greater increase in heart weight relative to body weight is observed compared to WT littermate females [28]. This finding suggests that estrogen receptor subtype beta plays a protective role in the development of pressure overload-induced cardiac hypertrophy and may be the mediator of observed sex differences.

We hypothesize that *Myh11*$^{E1892D/E1892D}$ SMCs in coronary arteries may produce a signal that alters the cardiomyocyte. We previously identified increased IGF-1 expression in aortic tissue of a patient with *MYH11* p.Leu1264Pro, another missense variant in the coiled-coil domain [8]. Transcriptomic analyses identified a 40-fold increase of *IGF1* expression in the SMCs explanted from the patient's aorta compared to SMCs explanted from normal aortas. Thus, *MYH11* rare variants may trigger excessive SMC IGF-1 production and be the source of SMC-to-cardiomyocyte signaling to drive cardiac hypertrophy and failure in *Myh11*$^{E1892D/E1892D}$ mice after TAC. One of the main pathways activated by IGF-1 is the PI3K/Akt/mTORC1 pathway that promotes protein synthesis and cell growth, contributing to cardiomyocyte hypertrophy in response to pressure overload. Inhibition of mTORC1 with rapamycin significantly attenuates cardiac hypertrophy and improves cardiac function with pressure overload [30, 31]. Activation of PI3K/Akt signaling could also lead to the phosphorylation and inactivation of the BCL2-associated agonist of cell death protein BAD and prevent oxidative stress-induced apoptotic death of cardiomyocytes, thereby enhancing cell survival [32]. Additionally, IGF-1 signaling promotes angiogenesis, ensuring adequate oxygen and nutrient supply to the hypertrophied myocardium and

246 supporting increased metabolic demands [33, 34]. However, if the underlying stress persists,
247 chronic activation and maladaptive remodeling can eventually lead to heart failure.

248 Another interesting finding in this study is that pressure overload leads to increased cardiac
249 fibrosis in the posterior wall of the *Myh11*$^{E1892D/E1892D}$ hearts, characterized by increased peri-
250 arterial and interstitial collagen deposition. Pressure overload-induced cardiac fibrosis is an
251 intricate process influenced by various molecular mechanisms, with activated fibroblasts and
252 myofibroblasts acting as the central effectors and serving as the main source of matrix proteins.
253 One key driver is the activation of the renin-angiotensin-aldosterone system due to decreased
254 stroke volume and renal blood flow [35], facilitating fibroblast proliferation and collagen
255 deposition in the myocardium [36, 37]. Increased biomechanical stress on the cardiac tissue leads
256 to release and activation of transforming growth factor-beta signaling, stimulating fibroblast
257 differentiation into myofibroblasts, which are responsible for excessive extracellular matrix
258 production [38, 39]. The activation of profibrotic pathways, such as the renin-angiotensin-
259 aldosterone system and transforming growth factor-beta signaling, is evident in TAC-induced
260 cardiac remodeling [37, 40]. Inflammatory responses mediated by cytokines and immune cells also
261 contribute to the progression of fibrosis post-TAC [37], while oxidative stress and mitochondrial
262 dysfunction have been implicated in TAC-induced cardiac fibrosis and dysfunction [41, 42].
263 Additionally, fibroblasts can also become activated by mechanical stress through
264 mechanosensitive receptors like integrins, ion channels, G-protein coupled receptors, and growth
265 factor receptors and can activate downstream signaling pathways that promote matrix production
266 [43]. Further studies will define the predominant signaling pathway that mediates the rapid
267 interstitial collagen deposition in male *Myh11*$^{E1892D/E1892D}$ mice.

Genome-wide association studies (GWAS) have identified loci involving *MYH11* associated with various traits of cardiac rhythm, including resting heart rate, heart rate response to exercise, atrial fibrillation, PR interval, and electrocardiography, suggesting a potential relationship between *MYH11* variants and cardiac pacing and arrhythmias. Additionally, three genetic risk loci (rs216158, rs9972711, rs12691049) encompassing *MYH11* have been linked to coronary artery disease [44]. Notably, no loci linked to *MYH11* have been associated with cardiac hypertrophy or heart failure in GWAS.

Collectively, these results demonstrate that a missense VUS in a gene almost exclusively expressed in SMCs, *MYH11*, does indeed increase thoracic aortic enlargement but also triggers aberrant pressure overload-induced remodeling of the heart that is characterized by increased cardiomyocyte hypertrophy, cardiac fibrosis, and heart failure in males. These findings provide further evidence of the diverse phenotypes associated with *MYH11* rare variants and implicate vascular SMC-to-cardiomyocyte signaling in driving aberrant cardiac remodeling with pressure overload. Future studies will focus on the interactions among different cell types in the heart and identify specific cellular pathways downstream of the mutant contractile protein in SMCs that mediate SMC-cardiomyocyte communications and contribute to cardiomyopathy.

Materials and Methods

Animal study

All animal experimental procedures were designed in accordance with National Institutes of Health guidelines and approved by the Animal Welfare Committee and the Center for Laboratory Animal Medicine and Care at the University of Texas Health Science Center at

Houston. *Myh11*$^{E1892D/+}$ breeders were transferred from the Jackson Laboratory and the colony was maintained on a C57BL/6J background.

Transverse aortic constriction surgery

At the age of 10-12 weeks, both male and female wild-type and *Myh11*$^{E1892D/E1892D}$ mice were anesthetized by 0.3-0.5 L/min pure oxygen with 2% isoflurane and placed supine on a 38°C heating pad. Intubation was performed with a 22-gauge venous catheter connected to a rodent ventilator with a respiratory rate of 125-150 breaths/min and a tidal volume of 6-8 μL/g. Carprofen (dose of 5 mg/kg, subcutaneous injection) and lidocaine (dose < 2.25 mg/kg, subcutaneous injection) were administrated before an upper partial sternotomy incision (about 1cm) was made. A 6-0 silk suture was coiled under the aortic arch between the innominate artery and the left common carotid artery and ligated with a 27-gauge needle placed by the aortic arch. The needle was then promptly removed to yield a constriction of 0.41mm in the outer diameter. The lungs were re-inflated before the skin was closed. Mice that died prior to the endpoint at fourteen days post-operation were subjected to necropsy to determine the cause of death. In male and female mice, comparable numbers succumbed following surgery (males: 2 out of 9 WT and 3 out of 10 mutants; females: 3 out of 10 WT and 2 out of 10 mutants). These expected post-operative mortality rates are primarily linked to acute congestive heart failure post-TAC [19], with the exception of one female that died due to coronary artery rupture (**S1 Fig** and **S1 Table**).

Echocardiography

Echocardiography (Vevo 3100 imaging system, MX550D transducer, VisualSonics, Toronto, Canada) was performed two weeks post-surgery. Briefly, mice were weighed and anesthetized by 0.5-1.0 L/min room air with 2% isoflurane via nose cone. Heart rate was closely monitored and body temperature was maintained around 38.5°C using the heating system. The

aortic root and ascending aorta were imaged in B-mode. Left ventricular function derived from short axis parasternal planes was imaged in M-mode. Measurements of maximal internal diameter of the proximal aorta and left ventricular contractile function were obtained from three different cardiac cycles and averaged. Data were analyzed by an operator blinded to the treatment groups.

Invasive blood pressure measurement

Following echocardiography analyses, intraluminal blood pressure measurements were performed using a Millar pressure catheter (SPR-1000, 1.0F, Oakville, Ontario, Canada) inserted into the right common carotid artery. Mice were intubated and placed on a ventilator using the same conditions as in TAC surgery except replacing pure oxygen with room air. The 1.0F catheter was inserted into the ascending aorta to monitor the blood pressure. Stable pressure tracings were recorded for 5 minutes at a PCU-2000 pressure signal conditioner and PowerLab 4/35 station (ADInstruments Inc., Colorado Springs, CO, USA), and systolic and diastolic blood pressures were averaged from the midterm 4 minutes record.

Myographic assay of aortic rings

Ascending aortic tissues were harvested from both male and female mice at the age of 10 months and delivered in ice-cold Hanks' Balanced Salt Solution through overnight shipping, and then cut into 2-mm ring segments and placed in the 620M Multi Chamber Myograph System (Danish Myo Technology, Hinnerup, Denmark) filled with 8 mL of oxygenated (95% O_2, 5% CO_2) physiological saline solution (118.31 mM NaCl, 4.69 mM KCl, 1.2 mM $MgSO_4$, 1.18 mM KH_2PO_4, 24.04 mM $NaHCO_3$, 0.02 mM EDTA, 2.5 mM $CaCl_2$, and 5.5 mM glucose) and allowed to equilibrate at 37 °C for at least 30 min. Aortic rings were stretched in 2-4 mN increments from 0 mN until the calculated transmural pressure reached 13.3 kPa (100 mmHg). Optimal resting tension was applied to the rings based on the passive vascular length-tension relationship.

Cumulative concentration-response curves to phenylephrine (PE, 10^{-9} to 10^{-5} M) and potassium chloride (KCl, 5-100 mM) were generated to assess contractile function. Vascular relaxation was assessed with acetylcholine (Ach, 10^{-9} to 10^{-5} M) and sodium nitroprusside (SNP, 10^{-9} to 10^{-5} M) administration. Concentration-response curves to Ach and sodium nitroprusside were generated after rings were pre-constricted to 70% of maximum with PE. Doses were added after the response curve reached a plateau from the previous dose. Percent vasocontractile responses (%) were calculated for PE and KCl as $[(D_P - D_B)/D_B] \times 100$, where '$D_P$' is the maximal force generated by a given specific dose and 'D_B' is the baseline force. Percent relaxation responses were calculated as $[(D_P - D_D)/ (D_P - D_B)] \times 100$, where D_P is the maximal force pre-generated by PE, D_D is the lowest force generated at a given dose of ACh or SNP and D_B is the baseline force [45, 46].

Histopathology

After intraperitoneal injection with Avertin (2.5%, 350 mg/kg), euthanized animals were perfusion fixed with 20 mL 1×PBS (pH=7.4) followed by 20 mL 10% neutral buffered formalin for 5 minutes through the left ventricle under physiological pressure. Ascending aortas and heart tissues were excised and further fixed in 10% neutral buffered formalin overnight at room temperature, then embedded in paraffin and sectioned at 5 μm. Aortic sections were stained with hematoxylin and eosin (H&E), Verhoeff Van Gieson (VVG, Polysciences, Inc., 25089-1), and Picro-Sirius Red (Abcam, ab150681) for morphometric analyses, medial elastic fibers and collagen content identification, respectively. Heart sections were stained with Picro-Sirius Red to determine collagen content. Images were obtained using a Leica DM2000 LED microscope, and analyzed with ImageJ software. Quantitative analyses were performed by 3 individuals blinded to the group information.

Wheat germ agglutinin staining

After rehydration, heart sections were stained with CF@640 dye WGA solution (Biotium, #29026-1) for 20 minutes at room temperature and protected from light, then mounted with DAPI (VECTASHIELD Antifade Mounting Medium, H-1200). Immunofluorescent images were obtained using the Leica DMi8 confocal microscope and analyzed with ImageJ software.

Immunoblot analyses

Proximal aortic tissue lysates were collected from ≥ 2 biological replicates per condition. Lysates were fractionated by SDS-PAGE and transferred to a polyvinylidene difluoride membrane according to standard protocols. Immunoblot images were quantitated with ImageJ software.

Statistical analysis

Data are presented as mean ± standard deviation. Nonparametric statistical tests were conducted. Statistical differences between two groups were analyzed using unpaired Mann-Whitney analysis. For three or more groups, Kruskal-Wallis analysis was performed, followed by Dunnett post-tests to compare between two specific groups. Analyses were performed using GraphPad Prism 9.0. Statistical significance was set at P-value < 0.05.

Acknowledgements

Study design, TAC surgery, echocardiography and blood pressure measurement, Western-blot assay, histology analyses, data analysis and discussion, and manuscript preparation, Z.Z.; Animal management, genotyping, echocardiography and blood pressure measurement, histology analyses, and discussion, K.H., N.S., P.P., and J. S.C.; Genetic data analysis and discussion, A.C.C., D.G., and D.R.M.; Myographic assay and discussion, H.K. and M.P.M.; Data analysis and discussion, M.Z. and J. W.; Patient consultation and discussion, J.M.G.; D.M.M. conceptualized

the project, secured funding, supervised the work, outlined and edited the manuscript. All authors read and approved the manuscript in its final form.

This research was funded by the Leducq Foundation, NIH HL146583, and private donations (D.M.M.). We would like to thank the family for participating in this study. We also grateful for the contributions of Nicholas Brown, Hongwei Jin, and the Center for Biometric Analysis at The Jackson Laboratory for expert assistance with this project.

References

1. Leguillette R, Lauzon AM. Molecular mechanics of smooth muscle contractile proteins in airway hyperresponsiveness and asthma. Proc Am Thorac Soc. 2008;5(1):40-6. Epub 2007/12/21. doi: 10.1513/pats.200704-053VS. PubMed PMID: 18094083.

2. Miano JM, Cserjesi P, Ligon KL, Periasamy M, Olson EN. Smooth muscle myosin heavy chain exclusively marks the smooth muscle lineage during mouse embryogenesis. Circ Res. 1994;75(5):803-12. Epub 1994/11/01. doi: 10.1161/01.res.75.5.803. PubMed PMID: 7923625.

3. Owens GK. Regulation of differentiation of vascular smooth muscle cells. Physiol Rev. 1995;75(3):487-517. Epub 1995/07/01. doi: 10.1152/physrev.1995.75.3.487. PubMed PMID: 7624392.

4. Manabe I, Owens GK. The smooth muscle myosin heavy chain gene exhibits smooth muscle subtype-selective modular regulation in vivo. J Biol Chem. 2001;276(42):39076-87. Epub 2001/08/08. doi: 10.1074/jbc.M105402200. PubMed PMID: 11489897.

5. Owens GK, Kumar MS, Wamhoff BR. Molecular regulation of vascular smooth muscle cell differentiation in development and disease. Physiol Rev. 2004;84(3):767-801. Epub 2004/07/23. doi: 10.1152/physrev.00041.2003. PubMed PMID: 15269336.

6. Chakraborty R, Saddouk FZ, Carrao AC, Krause DS, Greif DM, Martin KA. Promoters to Study Vascular Smooth Muscle. Arterioscler Thromb Vasc Biol. 2019;39(4):603-12. Epub 2019/02/08. doi: 10.1161/ATVBAHA.119.312449. PubMed PMID: 30727757; PubMed Central PMCID: PMCPMC6527360.

7. Zhu L, Vranckx R, Khau Van Kien P, Lalande A, Boisset N, Mathieu F, et al. Mutations in myosin heavy chain 11 cause a syndrome associating thoracic aortic aneurysm/aortic dissection and patent ductus arteriosus. Nat Genet. 2006;38(3):343-9. Epub 20060129. doi: 10.1038/ng1721. PubMed PMID: 16444274.

8. Pannu H, Tran-Fadulu V, Papke CL, Scherer S, Liu Y, Presley C, et al. MYH11 mutations result in a distinct vascular pathology driven by insulin-like growth factor 1 and angiotensin II. Hum Mol Genet. 2007;16(20):2453-62. Epub 2007/08/02. doi: 10.1093/hmg/ddm201. PubMed PMID: 17666408; PubMed Central PMCID: PMCPMC2905218.

9. Imai Y, Morita H, Takeda N, Miya F, Hyodo H, Fujita D, et al. A deletion mutation in myosin heavy chain 11 causing familial thoracic aortic dissection in two Japanese pedigrees. Int J Cardiol. 2015;195:290-2. Epub 20150603. doi: 10.1016/j.ijcard.2015.05.178. PubMed PMID: 26056961.
10. Yamasaki M, Abe K, Kosho T, Yamaguchi T. Familial Aortic Dissection in a Young Adult Caused by MYH11 Gene Mutation. Ann Thorac Surg. 2019;108(1):e49. Epub 2019/03/20. doi: 10.1016/j.athoracsur.2019.02.015. PubMed PMID: 30885847.
11. Chesneau B, Plancke A, Rolland G, Marcheix B, Dulac Y, Edouard T, et al. A +3 variant at a donor splice site leads to a skipping of the MYH11 exon 32, a recurrent RNA defect causing Heritable Thoracic Aortic Aneurysm and Dissection and/or Patent Ductus Arteriosus. Mol Genet Genomic Med. 2021;9(11):e1814. Epub 2021/10/22. doi: 10.1002/mgg3.1814. PubMed PMID: 34672437; PubMed Central PMCID: PMCPMC8606209.
12. Kuang SQ, Guo DC, Prakash SK, McDonald ML, Johnson RJ, Wang M, et al. Recurrent chromosome 16p13.1 duplications are a risk factor for aortic dissections. PLoS Genet. 2011;7(6):e1002118. Epub 2011/06/24. doi: 10.1371/journal.pgen.1002118. PubMed PMID: 21698135; PubMed Central PMCID: PMCPMC3116911.
13. Gauthier J, Ouled Amar Bencheikh B, Hamdan FF, Harrison SM, Baker LA, Couture F, et al. A homozygous loss-of-function variant in MYH11 in a case with megacystis-microcolon-intestinal hypoperistalsis syndrome. Eur J Hum Genet. 2015;23(9):1266-8. Epub 2014/11/20. doi: 10.1038/ejhg.2014.256. PubMed PMID: 25407000; PubMed Central PMCID: PMCPMC4538215.
14. Kloth K, Renner S, Burmester G, Steinemann D, Pabst B, Lorenz B, et al. 16p13.11 microdeletion uncovers loss-of-function of a MYH11 missense variant in a patient with megacystis-microcolon-intestinal-hypoperistalsis syndrome. Clin Genet. 2019;96(1):85-90. Epub 2019/05/03. doi: 10.1111/cge.13557. PubMed PMID: 31044419.
15. Gilbert MA, Schultz-Rogers L, Rajagopalan R, Grochowski CM, Wilkins BJ, Biswas S, et al. Protein-elongating mutations in MYH11 are implicated in a dominantly inherited smooth muscle dysmotility syndrome with severe esophageal, gastric, and intestinal disease. Hum Mutat. 2020;41(5):973-82. Epub 2020/01/17. doi: 10.1002/humu.23986. PubMed PMID: 31944481.
16. Kuang SQ, Kwartler CS, Byanova KL, Pham J, Gong L, Prakash SK, et al. Rare, nonsynonymous variant in the smooth muscle-specific isoform of myosin heavy chain, MYH11, R247C, alters force generation in the aorta and phenotype of smooth muscle cells. Circ Res. 2012;110(11):1411-22. Epub 2012/04/19. doi: 10.1161/CIRCRESAHA.111.261743. PubMed PMID: 22511748; PubMed Central PMCID: PMCPMC3917690.
17. Negishi K, Aizawa K, Shindo T, Suzuki T, Sakurai T, Saito Y, et al. An Myh11 single lysine deletion causes aortic dissection by reducing aortic structural integrity and contractility. Sci Rep. 2022;12(1):8844. Epub 20220525. doi: 10.1038/s41598-022-12418-8. PubMed PMID: 35614093; PubMed Central PMCID: PMCPMC9133116.
18. Zhou Z, Peters AM, Wang S, Janda A, Chen J, Zhou P, et al. Reversal of Aortic Enlargement Induced by Increased Biomechanical Forces Requires AT1R Inhibition in Conjunction With AT2R Activation. Arterioscler Thromb Vasc Biol. 2019;39(3):459-66. Epub 2019/01/04. doi: 10.1161/ATVBAHA.118.312158. PubMed PMID: 30602301; PubMed Central PMCID: PMCPMC6400319.

19. deAlmeida AC, van Oort RJ, Wehrens XH. Transverse aortic constriction in mice. J Vis Exp. 2010;(38). Epub 20100421. doi: 10.3791/1729. PubMed PMID: 20410870; PubMed Central PMCID: PMCPMC3164086.

20. Bensley JG, De Matteo R, Harding R, Black MJ. Three-dimensional direct measurement of cardiomyocyte volume, nuclearity, and ploidy in thick histological sections. Sci Rep. 2016;6:23756. Epub 2016/04/07. doi: 10.1038/srep23756. PubMed PMID: 27048757; PubMed Central PMCID: PMCPMC4822151.

21. Huet C, Garrido J. Ultrastructural visualization of cell-coat components by means of wheat germ agglutinin. Exp Cell Res. 1972;75(2):523-7. Epub 1972/12/01. doi: 10.1016/0014-4827(72)90463-6. PubMed PMID: 4674699.

22. Rockman HA, Ross RS, Harris AN, Knowlton KU, Steinhelper ME, Field LJ, et al. Segregation of atrial-specific and inducible expression of an atrial natriuretic factor transgene in an in vivo murine model of cardiac hypertrophy. Proc Natl Acad Sci U S A. 1991;88(18):8277-81. doi: 10.1073/pnas.88.18.8277. PubMed PMID: 1832775; PubMed Central PMCID: PMCPMC52490.

23. Wu D SY, Li C, Xiao L, Dai J, Chen Y, Chen P, Wang H, Yu B, Wei H, Li R, Song X, Yu T, Shi L, Wang DW. Rare variants in the FBN1 gene are associated with sporadic dilated cardiomyopathy in a Chinese Han population. J Cardiovasc Aging. 2023;3(3):30. doi: 10.20517/jca.2023.12.

24. Zi M, Stafford N, Prehar S, Baudoin F, Oceandy D, Wang X, et al. Cardiac hypertrophy or failure? - A systematic evaluation of the transverse aortic constriction model in C57BL/6NTac and C57BL/6J substrains. Curr Res Physiol. 2019;1:1-10. doi: 10.1016/j.crphys.2019.10.001. PubMed PMID: 32699840; PubMed Central PMCID: PMCPMC7357793.

25. Williams JL, Paudyal A, Awad S, Nicholson J, Grzesik D, Botta J, et al. Mylk3 null C57BL/6N mice develop cardiomyopathy, whereas Nnt null C57BL/6J mice do not. Life Sci Alliance. 2020;3(4). Epub 20200325. doi: 10.26508/lsa.201900593. PubMed PMID: 32213617; PubMed Central PMCID: PMCPMC7103425.

26. Richards DA, Aronovitz MJ, Calamaras TD, Tam K, Martin GL, Liu P, et al. Distinct Phenotypes Induced by Three Degrees of Transverse Aortic Constriction in Mice. Sci Rep. 2019;9(1):5844. Epub 20190410. doi: 10.1038/s41598-019-42209-7. PubMed PMID: 30971724; PubMed Central PMCID: PMCPMC6458135.

27. Wang X, Zhu X, Shi L, Wang J, Xu Q, Yu B, et al. A time-series minimally invasive transverse aortic constriction mouse model for pressure overload-induced cardiac remodeling and heart failure. Front Cardiovasc Med. 2023;10:1110032. Epub 20230220. doi: 10.3389/fcvm.2023.1110032. PubMed PMID: 36891245; PubMed Central PMCID: PMCPMC9986492.

28. Skavdahl M, Steenbergen C, Clark J, Myers P, Demianenko T, Mao L, et al. Estrogen receptor-beta mediates male-female differences in the development of pressure overload hypertrophy. Am J Physiol Heart Circ Physiol. 2005;288(2):H469-76. Epub 20040916. doi: 10.1152/ajpheart.00723.2004. PubMed PMID: 15374829.

29. Witt H, Schubert C, Jaekel J, Fliegner D, Penkalla A, Tiemann K, et al. Sex-specific pathways in early cardiac response to pressure overload in mice. J Mol Med (Berl). 2008;86(9):1013-24. Epub 20080730. doi: 10.1007/s00109-008-0385-4. PubMed PMID: 18665344; PubMed Central PMCID: PMCPMC2517094.

30. Shioi T, McMullen JR, Tarnavski O, Converso K, Sherwood MC, Manning WJ, et al. Rapamycin attenuates load-induced cardiac hypertrophy in mice. Circulation. 2003;107(12):1664-70. Epub 20030317. doi: 10.1161/01.CIR.0000057979.36322.88. PubMed PMID: 12668503.
31. McMullen JR, Sherwood MC, Tarnavski O, Zhang L, Dorfman AL, Shioi T, et al. Inhibition of mTOR signaling with rapamycin regresses established cardiac hypertrophy induced by pressure overload. Circulation. 2004;109(24):3050-5. Epub 20040607. doi: 10.1161/01.CIR.0000130641.08705.45. PubMed PMID: 15184287.
32. Aikawa R, Nawano M, Gu Y, Katagiri H, Asano T, Zhu W, et al. Insulin prevents cardiomyocytes from oxidative stress-induced apoptosis through activation of PI3 kinase/Akt. Circulation. 2000;102(23):2873-9. doi: 10.1161/01.cir.102.23.2873. PubMed PMID: 11104747.
33. Nakao-Hayashi J, Ito H, Kanayasu T, Morita I, Murota S. Stimulatory effects of insulin and insulin-like growth factor I on migration and tube formation by vascular endothelial cells. Atherosclerosis. 1992;92(2-3):141-9. doi: 10.1016/0021-9150(92)90273-j. PubMed PMID: 1378740.
34. Chen L, Samanta A, Zhao L, Dudley NR, Buehler T, Vincent RJ, et al. Vitamin D3 induces mesenchymal-to-endothelial transition and promotes a proangiogenic niche through IGF-1 signaling. iScience. 2021;24(4):102272. Epub 20210304. doi: 10.1016/j.isci.2021.102272. PubMed PMID: 33817577; PubMed Central PMCID: PMCPMC8005757.
35. Wesseling M, Mulder E, Brans MAD, Kapteijn DMC, Bulthuis M, Pasterkamp G, et al. Mildly Increased Renin Expression in the Absence of Kidney Injury in the Murine Transverse Aortic Constriction Model. Front Pharmacol. 2021;12:614656. Epub 20210615. doi: 10.3389/fphar.2021.614656. PubMed PMID: 34211391; PubMed Central PMCID: PMCPMC8239225.
36. AlQudah M, Hale TM, Czubryt MP. Targeting the renin-angiotensin-aldosterone system in fibrosis. Matrix Biol. 2020;91-92:92-108. Epub 20200516. doi: 10.1016/j.matbio.2020.04.005. PubMed PMID: 32422329; PubMed Central PMCID: PMCPMC7434656.
37. Frangogiannis NG. Cardiac fibrosis. Cardiovasc Res. 2021;117(6):1450-88. doi: 10.1093/cvr/cvaa324. PubMed PMID: 33135058; PubMed Central PMCID: PMCPMC8152700.
38. Weber KT, Sun Y, Bhattacharya SK, Ahokas RA, Gerling IC. Myofibroblast-mediated mechanisms of pathological remodelling of the heart. Nat Rev Cardiol. 2013;10(1):15-26. Epub 20121204. doi: 10.1038/nrcardio.2012.158. PubMed PMID: 23207731.
39. Rosenkranz S. TGF-beta1 and angiotensin networking in cardiac remodeling. Cardiovasc Res. 2004;63(3):423-32. doi: 10.1016/j.cardiores.2004.04.030. PubMed PMID: 15276467.
40. Frangogiannis NG. Transforming growth factor-beta in myocardial disease. Nat Rev Cardiol. 2022;19(7):435-55. Epub 20220104. doi: 10.1038/s41569-021-00646-w. PubMed PMID: 34983937.
41. Lu Z, Xu X, Hu X, Fassett J, Zhu G, Tao Y, et al. PGC-1 alpha regulates expression of myocardial mitochondrial antioxidants and myocardial oxidative stress after chronic systolic overload. Antioxid Redox Signal. 2010;13(7):1011-22. doi: 10.1089/ars.2009.2940. PubMed PMID: 20406135; PubMed Central PMCID: PMCPMC2959178.
42. Peoples JN, Saraf A, Ghazal N, Pham TT, Kwong JQ. Mitochondrial dysfunction and oxidative stress in heart disease. Exp Mol Med. 2019;51(12):1-13. Epub 20191219. doi:

10.1038/s12276-019-0355-7. PubMed PMID: 31857574; PubMed Central PMCID: PMCPMC6923355.

43. Barnes LA, Marshall CD, Leavitt T, Hu MS, Moore AL, Gonzalez JG, et al. Mechanical Forces in Cutaneous Wound Healing: Emerging Therapies to Minimize Scar Formation. Adv Wound Care (New Rochelle). 2018;7(2):47-56. doi: 10.1089/wound.2016.0709. PubMed PMID: 29392093; PubMed Central PMCID: PMCPMC5792236.

44. Koyama S, Ito K, Terao C, Akiyama M, Horikoshi M, Momozawa Y, et al. Population-specific and trans-ancestry genome-wide analyses identify distinct and shared genetic risk loci for coronary artery disease. Nat Genet. 2020;52(11):1169-77. Epub 20201005. doi: 10.1038/s41588-020-0705-3. PubMed PMID: 33020668.

45. Holly D, Kim H, Woodman CR, Massett MP. Genetic background influences arterial vasomotor function in male and female mice. Physiol Rep. 2023;11(19):e15824. doi: 10.14814/phy2.15824. PubMed PMID: 37771071; PubMed Central PMCID: PMCPMC10539628.

46. Ojha KR, Kim H, Padgham S, Hopkins L, Zamen RJ, Chattopadhyay A, et al. Smooth Muscle-Alpha Actin R149C Pathogenic Variant Downregulates Integrin Recruitment at Cell-Matrix Adhesions and Decreases Cellular Contractility. Int J Mol Sci. 2023;24(11). Epub 20230601. doi: 10.3390/ijms24119616. PubMed PMID: 37298565; PubMed Central PMCID: PMCPMC10253315.

Supporting information

Fig 1. Cardiovascular phenotyping in wild-type (WT) and *Myh11*$^{E1892D/E1892D}$ mice. (A) Sequencing of DNA sample from tail tissue and cDNA sample from both heart and aorta confirms single nucleotide variant in mouse *Myh11 gene*. **(B)** Tail-cuff blood pressure measurement. **(C)** and **(D)** Echocardiographic measurements of aortic root, ascending aorta, and left ventricular contractile function. N=10 in each group. SBP, systolic blood pressure, DBP, diastolic blood pressure, ASC, ascending aorta. * P<0.05.

Fig 2. Assessment of myograph and smooth muscle cell contractile protein expression in ascending aortic tissues. (A) Myographic assay of mouse ascending aortic rings at 10 months of age. N=4 (3M+1F) in each group. **(B)** Immunoblot assay of protein lysates of the ascending aortas from wild-type (WT), heterozygous (HET), and homozygous (HOMO) mice at the age of 6 months.

N=2, 5, 2 in the WT, HET, and HOMO group, respectively. KCl, potassium chloride; PE, phenylephrine; Ach, acetylcholine; SNP, sodium nitroprusside.

Fig 3. Assessment of ascending aortic remodeling 2 weeks after transverse aortic constriction (TAC) in male mice. (A) Representative images of proximal aortic ultrasound measurement, H&E, VVG, and Sirius Red staining on ascending aortic tissue sections. **(B)** TAC induces similar levels of systolic (SBP) and diastolic (DBP) blood pressure in wild-type (WT) and *Myh11*$^{E1892D/E1892D}$ mice, along with significant ascending aortic enlargement in *Myh11*$^{E1892D/E1892D}$ mice. **(C)** Histology analysis shows significantly increased medial thickening and elastic breaks in the mutant aortas compare with WT TAC aortas, with no difference of adventitial area or collagen accumulation. ns, non-significant; * P<0.05. ● WT TAC, ■ *Myh11*$^{E1892D/E1892D}$ TAC.

Fig 4. Assessment of left ventricular remodeling 2 weeks after transverse aortic constriction (TAC) in male mice. (A) Representative images of left ventricular (LV) contraction using M-mode. **(B)** Four functional parameters show decreased LV contractility in *Myh11*$^{E1892D/E1892D}$ mice 2 weeks after TAC. **(C)** Structural parameters of LV show increased end diastole (d) and systole (s) thickness of posterior wall (PW), along with increased LV diameters and volumes in *Myh11*$^{E1892D/E1892D}$ mice after TAC. **(D)** Wheat Germ Agglutinin (WGA) staining of LVPW shows significant increase of cardiomyocyte cross section area in male *Myh11*$^{E1892D/E1892D}$ heart after TAC. **(E)** Representative images of Sirius Red staining of LVPW. Quantification of collagen deposition area shows increased peri-arterial (left circumflex artery, LCX) area and LVPW collagen density in *Myh11*$^{E1892D/E1892D}$ heart after TAC. ns, non-significant; * P<0.05, ** P<0.01, *** P<0.001. ● WT TAC, ■ *Myh11*$^{E1892D/E1892D}$ TAC.

S1 Fig. Necropsy of a mouse died one day after transverse aortic constriction. One *Myh11*$^{E1892D/E1892D}$ female mouse died of ruptured left main coronary artery and associated cardiac tamponade one day after TAC. Yellow arrow and a 5-0 suture show the rupture site.

S2 Fig. Echocardiography and central blood pressure measurements 2 weeks after transverse aortic constriction (TAC) in female mice. **(A)** Aortic root and ascending (ASC) aortic diameters. **(B)** Systolic (SBP) and diastolic (DBP) blood pressures. **(C)** Evaluation of left ventricular (LV) contractile function in female mice after TAC. **(D)** Structural evaluation of LV in female mice after TAC. AW, anterior wall; PW, posterior wall; d, end diastolic; s, end systolic; ns, non-significant; * P<0.05.

S3 Fig. Wheat Germ Agglutinin (WGA) staining of left ventricular anterior wall (LVAW). There is no difference of cardiomyocyte cross-sectional area between male wild-type and *Myh11*$^{E1892D/E1892D}$ mice after TAC. ns, non-significant. ● WT TAC, ■ *Myh11*$^{E1892D/E1892D}$ TAC.

S4 Fig. Comparison of left ventricular contractile function between male and female mutant mice 2 weeks after transverse aortic constriction (TAC). Male *Myh11*$^{E1892D/E1892D}$ mice exhibit significantly lower ejection fraction and fractional shortening compared to female mutant mice following TAC. ns, non-significant; ** P<0.01.

S1 Table. Total numbers of mice died after transverse aortic constriction.

S2 Table. Segregation record of 102 progenies from heterozygous breeders.

Fig 1.

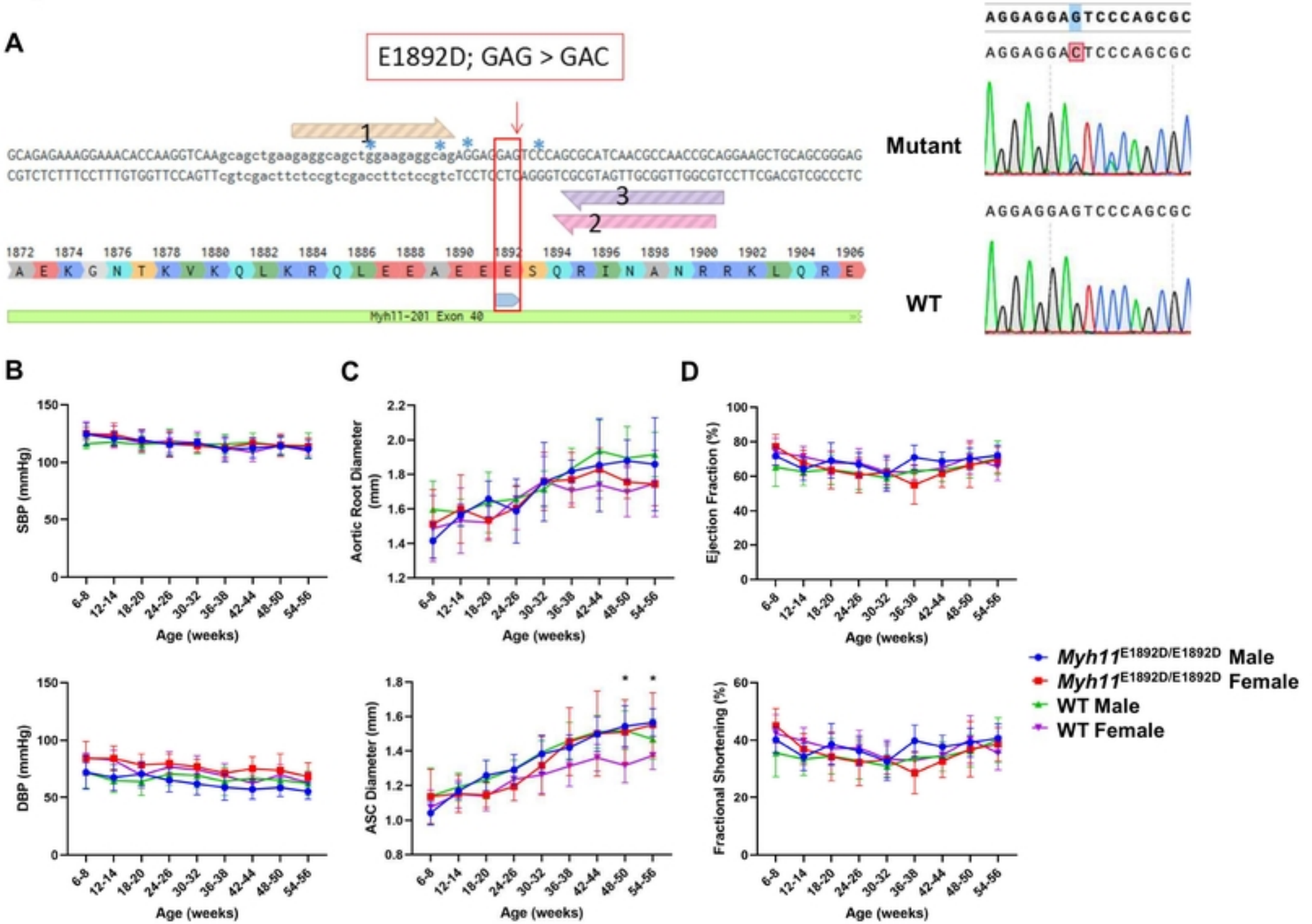
A
E1892D; GAG > GAC
GCAGAGAAAGGAAACACCAAGGTCAAgcagctgaagaggcagctggaagaggcagAGGAGGAGTCCCAGCGCATCAACGCCAACCGCAGGAAGCTGCAGCGGGAG
CGTCTCTTTCCTTTGTGGTTCCAGTTcgtcgacttctccgtcgaccttctccgtcTCCTCCTCAGGGTCGCGTAGTTGCGGTTGGCGTCCTTCGACGTCGCCCTC
1872 1874 1876 1878 1880 1882 1884 1886 1888 1890 1892 1894 1896 1898 1900 1902 1904 1906
A E K G N T K V K Q L K R Q L E E A E E E S Q R I N A N R R K L Q R E
Myh11-201 Exon 40
Mutant
WT
AGGAGGAGTCCCAGCGC
AGGAGGACTCCCAGCGC
AGGAGGAGTCCCAGCGC
B
C
D
SBP (mmHg)
DBP (mmHg)
Aortic Root Diameter (mm)
ASC Diameter (mm)
Ejection Fraction (%)
Fractional Shortening (%)
Age (weeks)
6-8
12-14
18-20
24-26
30-32
36-38
42-44
48-50
54-56
Myh11E1892D/E1892D Male
Myh11E1892D/E1892D Female
WT Male
WT Female

Fig 1

Fig 2.

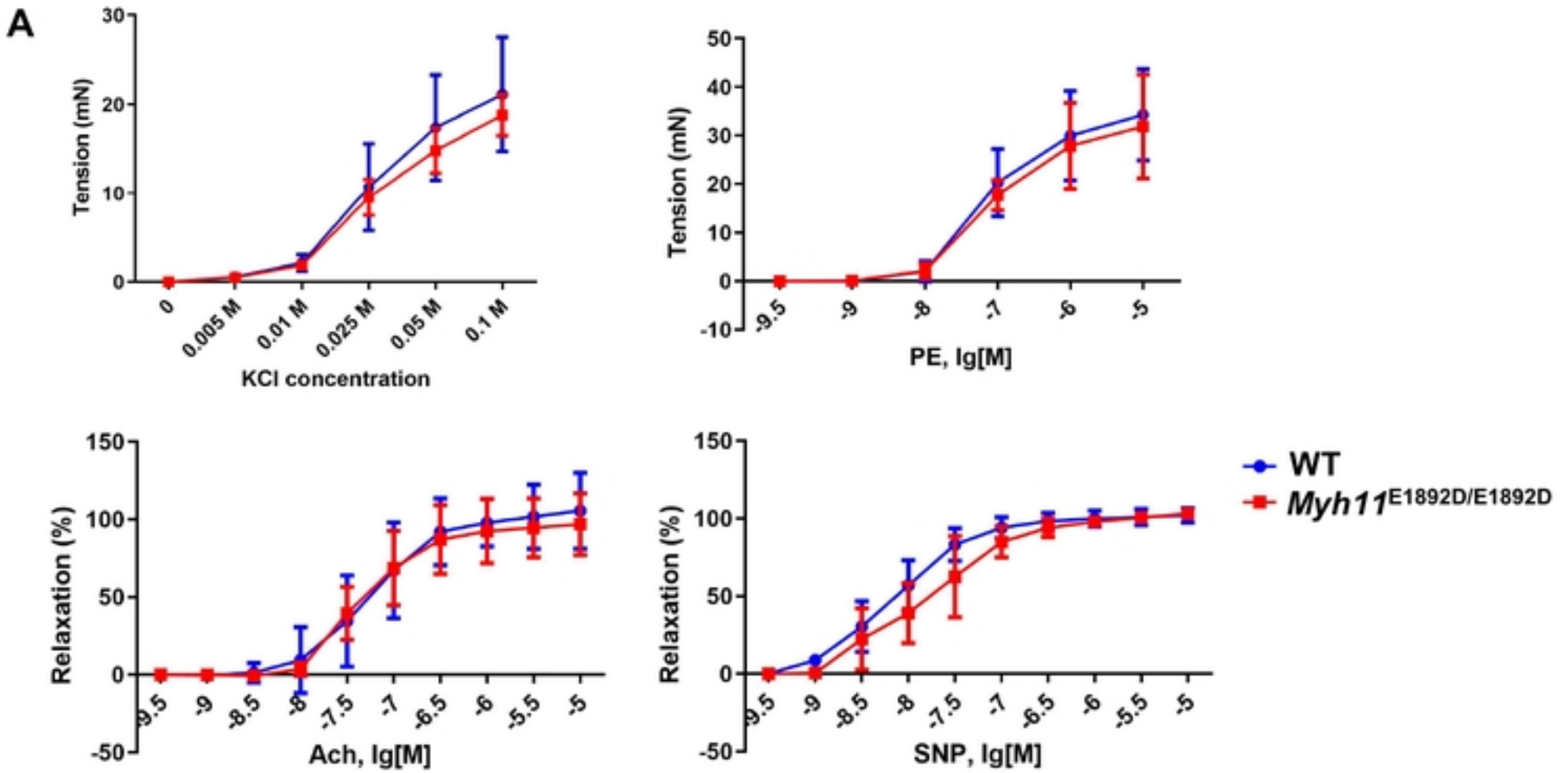

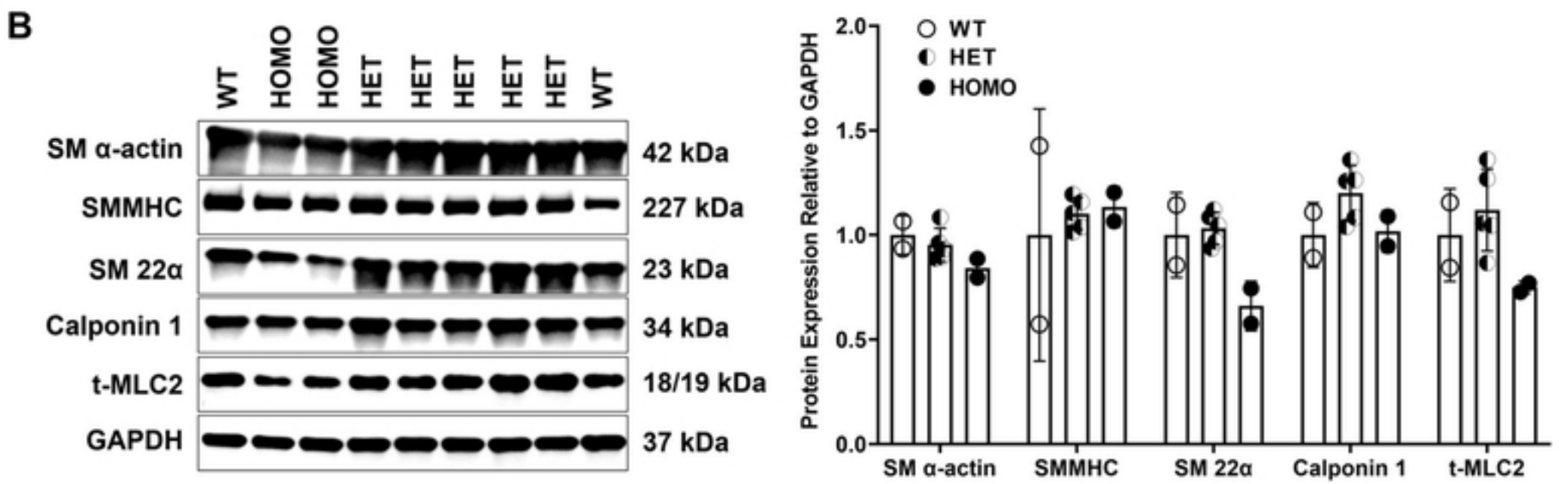

Fig 2

Fig 3.

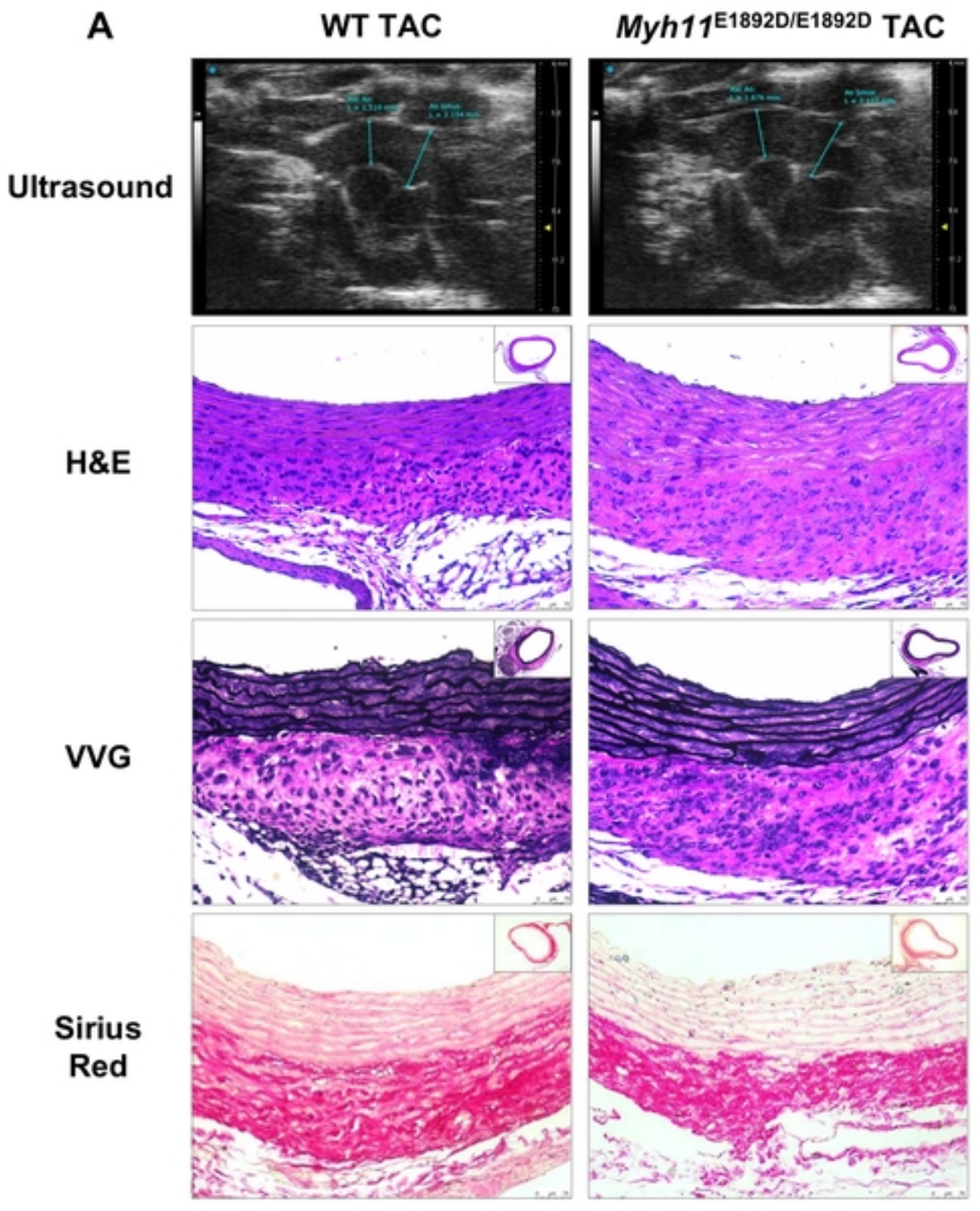

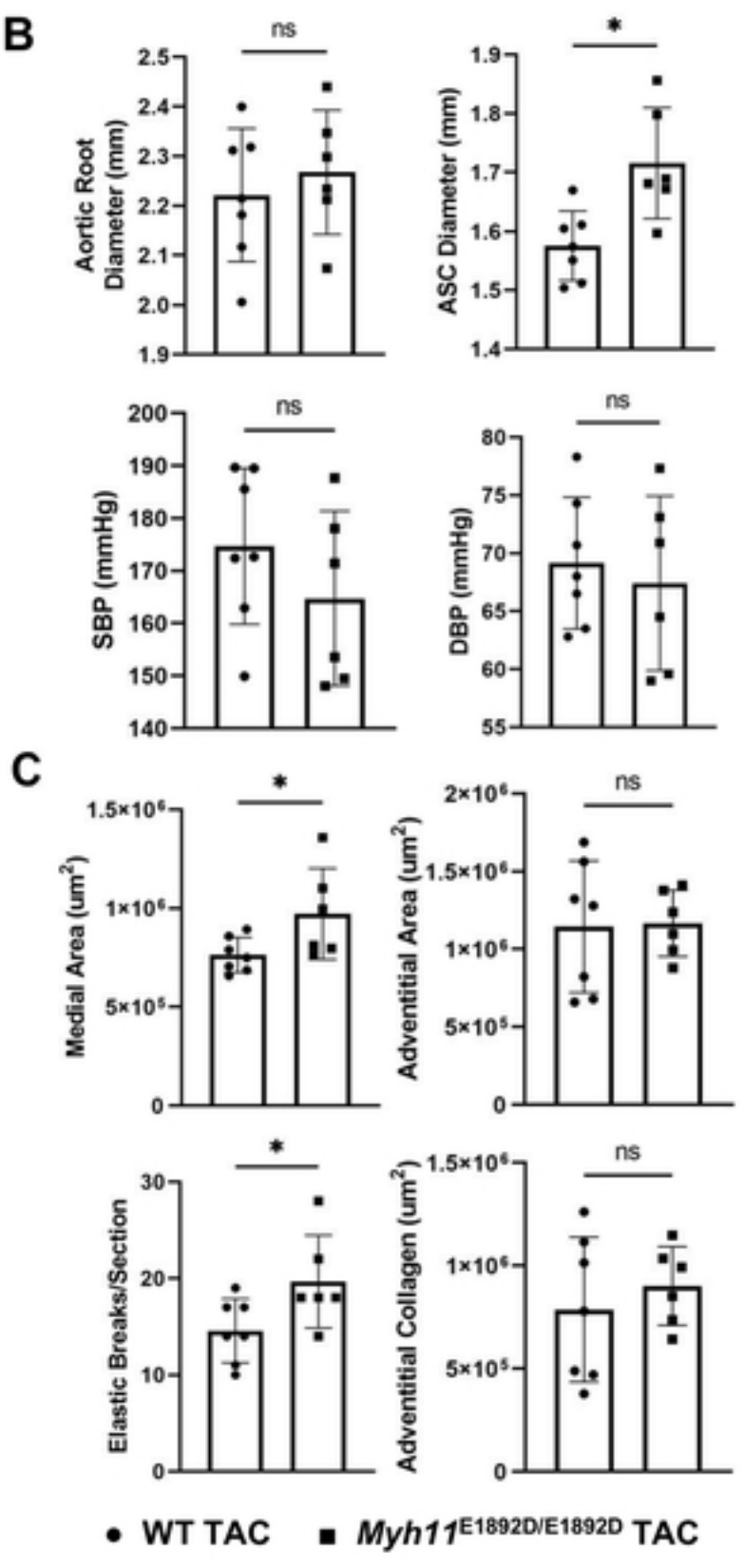

Fig 3

Fig 4.

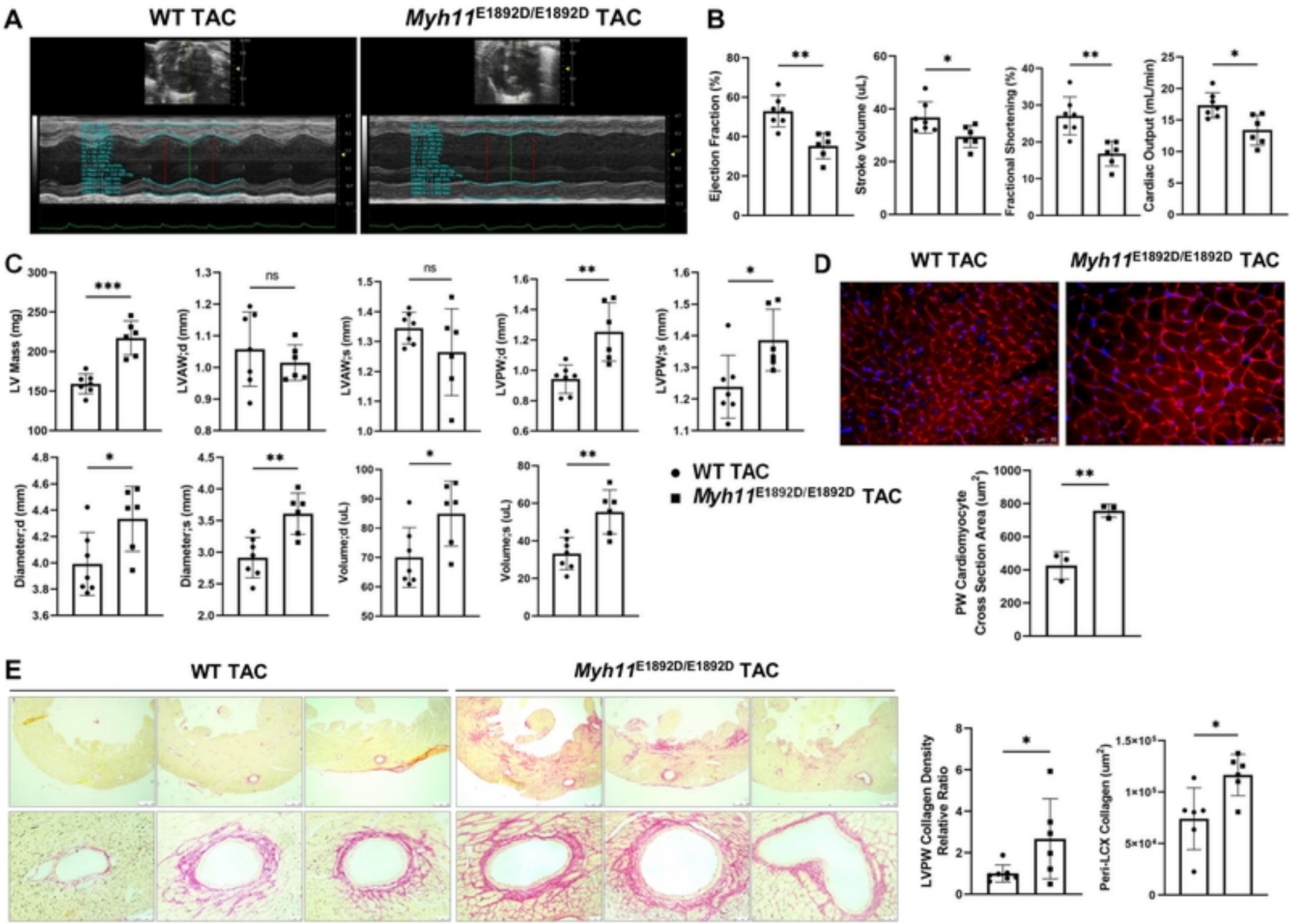
A
WT TAC
Myh11E1892D/E1892D TAC
B
Ejection Fraction (%)
Stroke Volume (uL)
Fractional Shortening (%)
Cardiac Output (mL/min)
C
LV Mass (mg)
LVAW;d (mm)
LVAW;s (mm)
LVPW;d (mm)
LVPW;s (mm)
Diameter;d (mm)
Diameter;s (mm)
Volume;d (uL)
Volume;s (uL)
ns
WT TAC
Myh11E1892D/E1892D TAC
D
WT TAC
Myh11E1892D/E1892D TAC
PW Cardiomyocyte Cross Section Area (um2)
E
WT TAC
Myh11E1892D/E1892D TAC
LVPW Collagen Density Relative Ratio
Peri-LCX Collagen (um2)

Fig 4